Detector Overview ___ focused on interaction region

Toshiaki Tauchi
KEK,High Energy Accelerator Research Organization,
1-1 Oho, Tsukuba-shi,Ibaraki-ken, 305-0810, Japan.

Abstract

Briefly describing characteristics of beam, background related to the beam and the interaction region at the e^+e^- linear collider JLC, we compare three detectors proposed for JLC, NLC and TESLA. Finally, we list issues to be discussed at a series of the ACFA workshops.

1 Characteristics of beams at JLC

JLC is an e^+e^- linear collider at a TeV energy region. The center-of-mass energy is $250 < \sqrt{s} < 500$GeV at the first phase[1], and it will be extended more then 1 TeV in the next phase[2]. The JLC consists of three major systems of pre-acceleration, main acceleration and final focus as shown in Fig.1[3]. The pre-acceleration system produces a high quality beam to be

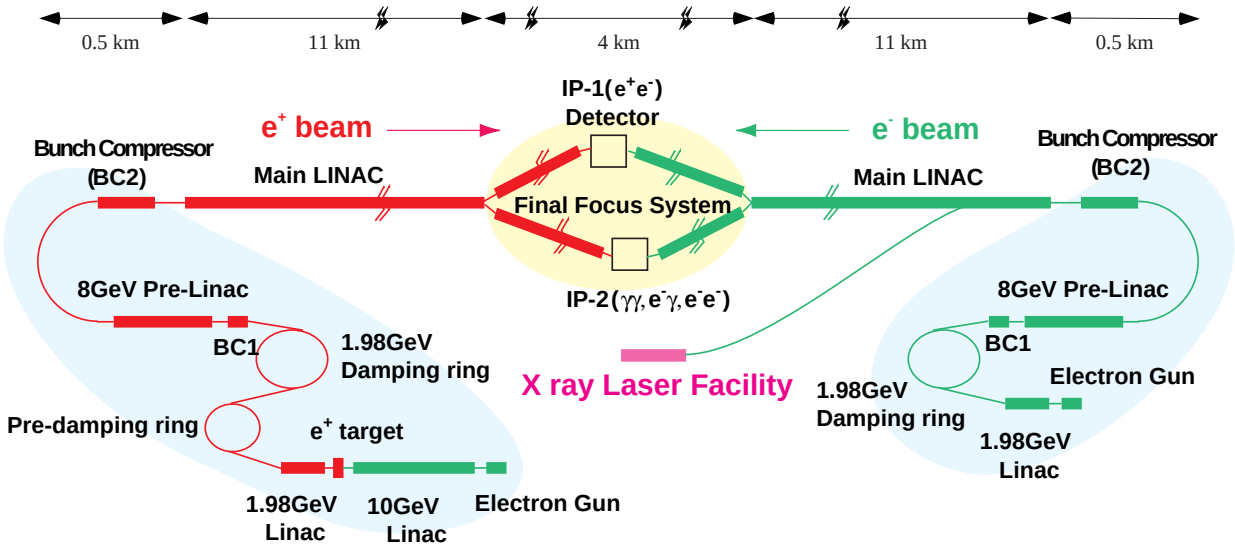

Figure 1: Schematics of JLC accelerator complex ($0.25\text{TeV} < \sqrt{s_{e^+e^-}} < 1.0\text{TeV}$) .

injected into the main linear accelerator(linac). First, a high intensity beam(7.0×10^9/bunch) is created with a multi-bunch structure (85 bunches/RF pulse) by a thermionic-electron gun at 150Hz. In a 1.98GeV damping ring, the emittance of the beam is reduced so that the divergence times the cross section of the beam shrinks by about 1/100 of what has been achieved

Table 1: JLC parameters based on x-band main LINAC of JLC Design Study, April 1997. The numbers are those with crab crossing. Luminosities are 3.15, 5.18, $7.66\times10^{33}\mathrm{cm}^{-2}\mathrm{s}^{1}$ at $\sqrt{s}$=250, 500 and 1000 GeV, respectively, without crab crossing.

RF frequency	11.4 GHz (λ=2.6 cm)
no. of electrons/bunch	7.0×10^9 (6.45×10^9 at IP)
no. of bunches/train	85
bunch separation	1.4 nsec
accelerating gradient	55.6 MeV/m (loaded)
normalized emittance	3(H) / 0.03(V) 10^{-6} rad m LINAC
	3.3(H) / 0.048(V) 10^{-6} rad m IP
horizontal crossing angle	8 mrad

	$\sqrt{s}$=250GeV	500 GeV	1.0 TeV	
no. of klystrons/beam	1053	2197	4485	
AC power(wall plug) assuming 28% efficiency	55	115	234	MW
repetition rate	150	150	150	Hz
β_x^*/β_y^*	10/100	10/100	10/100	mm/μm
σ_x^*/σ_y^*	367/4.43	260/3.14	184/2.28	nm/nm
$\Delta E/E$ due to beamstrahlung	1.34	3.40	6.90	%
pinch enhancement	1.581	1.585	1.599	
luminosity	4.13	8.28	16.72	$\times10^{33}$ $\mathrm{cm}^{-2}\mathrm{s}^{1}$

so far. At the positron beam line, there are an additional 10 GeV electron-linac to create positrons at e^+ target and a pre-damping ring with a large positron capture efficiency. The bunch length of the beam is compressed from ∼5mm to ∼0.1mm by bunch compressors in order to be efficiently accelerated at the main linac. In the main acceleration system (main linac), the beam is accelerated with the average gradient of 55.6MeV/m by a 11.4GHz(x-band) RF system consisting of klystrons and accelerating cavities. Collimating the beam to control beam-related backgrounds at the interaction point, the beam is strongly focussed to 3nm(σ_y) and 260nm(σ_x) in vertical and horizontal directions, respectively, in the final focus system. The design luminosity is $8.28 \times 10^{33}\mathrm{cm}^{-2}\mathrm{sec}^{-1}$ at $\sqrt{s}$=500GeV. There are two interaction points with their own final focus systems. The motivation of the second interaction point is for $\gamma\gamma$, $e^-\gamma$, and e^-e^- collisions for complementary physics to e^+e^-[4]. Also, JLC may have an X ray laser facility for material physics[1].

Major parameters are listed in table 1. To provide high luminosity with a relatively low repetition rate of 150Hz, the beam is strongly focussed especially in vertical direction and it has a bunch-train structure, as shown in Figures 2 and 3, respectively. One train consists of 85 bunches. The bunches are separated with 1.4nsec in each. The luminosity per bunch is still high, that is several$\times10^{29}\mathrm{cm}^{-2}$/bunch. So, there may have a possibility of signal overlapping with background processes within a train collision if the event can not be resolved into a specific bunch collision. Therefore, it is desirable for detectors to have good time resolutions of an order of nano-second. Contrary, the low repetition rate may simplify a trigger scheme without any

Figure 2: Transverse profile of the beam.

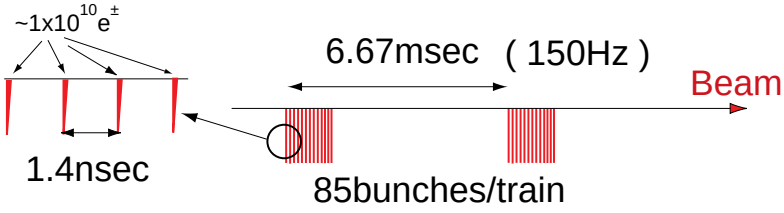

Figure 3: Bunch-train structure of the beam.

hardware trigger. All the data can be read-out at 150Hz, then the interesting events can be discriminated with software trigger in every interval of 6.6msec.

2 Backgrounds related to beams

To illustrate where the background particles can originate, the beam line from the exit of the main linear accelerator (linac) to the interaction point (IP) is schematically shown in Figure 4. A +7 mrad bending magnet section (200 m long) downstream of the collimation section is needed in order to create a sufficient amount of separation for two experimental halls and to prevent the background from the upstream linac from directly hitting the detector. In the final focus system, beams are gradually deflected so as to have a horizontal beam crossing angle of ±4 mrad at the interaction point (IP). There are two major sections for beam collimation (1200 m long) and a final focus system(1800m long) in the beam line to handle beam energies up to 0.75 TeV. While their main purposes are to clip the beam tails, secondary particles are inevitably produced, namely: (1) muons and (2) synchrotron radiation photons, respectively. In addition at the IP, (3) e^+e^- pairs and (4) mini-jet are created through beam-beam interactions. They all cause background hits in the detector facility.

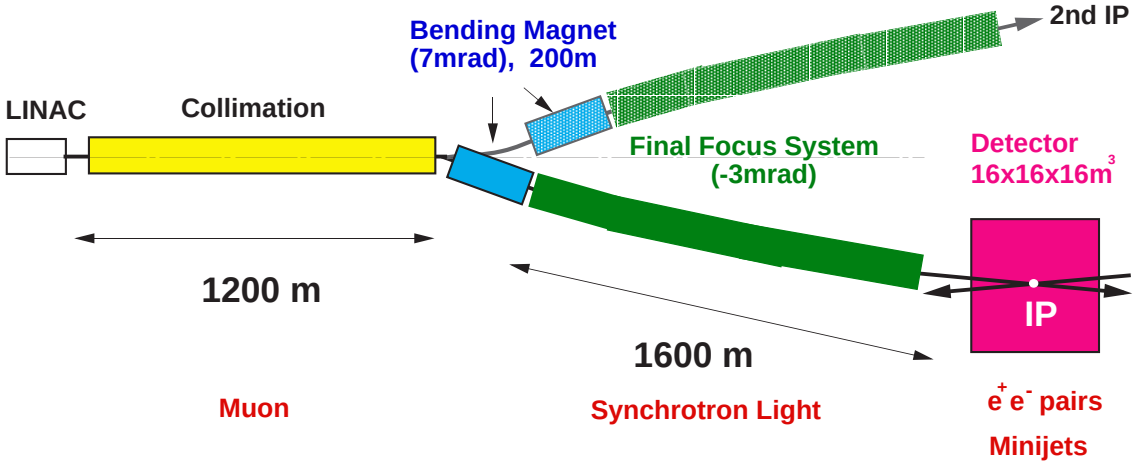

Figure 4: Schematics of beam delivery system at $\sqrt{s}$ <1.5TeV .

Assuming a 1% flat tail beyond $3\sigma_{x,y}$, about 10^{10} electrons must be collimated for a single train crossing. Without any muon-shield, 10^5 muons/train may penetrate a detector of $16\times16\text{m}^3$

volume. Recent study shows that the beam line between 1510 and 2856m from the IP must be covered with magnetized iron pipes of 30cm outer radius, so called muon attenuators, in order to achieve a suppression factor of $> 10^{-5}$, where only 1 muon/train can penetrate the detector[5].

The collimated beam size has been optimized to be $6\sigma_x \times 40\sigma_y$ in order to control synchrotron radiations emitted in the final focus system. Thus well-collimated synchrotron radiations can pass through the nearest final quadrupole magnet without scattering as shown in Figure 5.

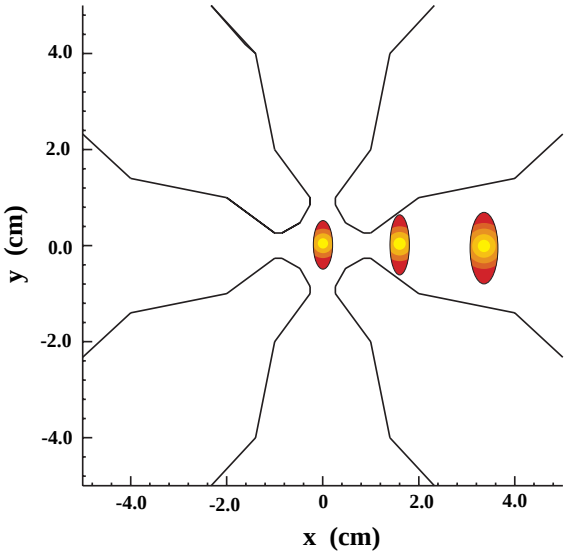

Figure 5: Profiles of synchrotron radiations at the nearest quadrupole magnet(QC1), which is located at 2m from the interaction point, together with the pole tips of QC1. The profile at the center accompanies the incoming beam. Two right hand side ones are passing through QC1 of 2.2 m long with 8 mrad horizontal crossing.

When two beams collide at the interaction point (IP), a huge number of low energy e^+e^- pairs are produced in three processes of $e^+e^- \to e^+e^-e^+e^-$, $\gamma e^\pm \to e^+e^-e^\pm$ and $\gamma\gamma \to e^+e^-$ ($\gamma \equiv$ beamstrahlung photon). Since their cross sections are orders of $10^{-25} \sim 10^{-27}$ cm^{-2}, about 10^5 pairs must be created per bunch crossing. Although the typical scattering angle is $1/\gamma \equiv m_e/E$, the low energy electrons/positrons can be largely kicked out from the beam line by the strong magnetic field produced by coming beam as shown in Figure 6. Since the kick angles are large enough for them to hit the pole tips of QC1, they produce a lot of showered particles. A large fraction of them may also penetrate a vertex detector located at a few cm from the beam line. In a magnetic field of detector-solenoid (2 tesla), low energy photons (X rays) are most severe backgrounds among the showered particles. During depositing energies in the shower, neutrons are also produced from photo-excited nuclei. The typical rate is 1 neutron per 0.13GeV energy deposit in iron. So, a rough estimation shows that 10^{15} neutrons may be produced per year. The effects of these particles on detectors need a detailed simulation study. In the next section, one configuration of the interaction region is explained against the X rays.

In addition to the e^+e^- pairs, there are jets productions in two photon process, so called mini-jets, of $\gamma\gamma \to q\bar{q}$ where γ is a virtual or beamstrahlung photon. The production cross section strongly depends on the model of hadronic structure of a photon as well as the minimum transverse momentum of quarks. The first estimations ranged from 0.06 to 0.2 events per

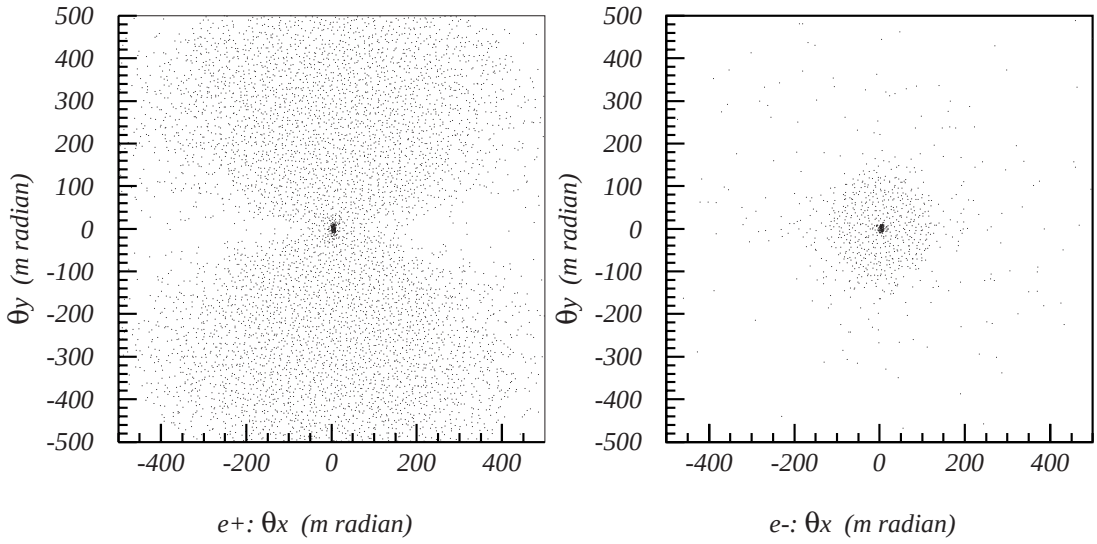

Figure 6: Kicked angles of low energy electrons/positrons. The vertical and horizontal axes denote the kicked angles in vertical and horizontal directions, respectively. The left and right figures show distributions of the positrons and the electrons, respectively, downstream of the electron beam. Since the positrons have the same sign charge as the in-coming (positron) beam, they are scattered by larger angles than the electrons.

bunch crossing at $\sqrt{s}$=0.5 TeV[6]. So, a good time resolution of O(nsec)is very important to discriminate a signal from minijets.

3 Interaction region

A possible configuration of the interaction region is shown in Figure 7. A cone-shaped mask of heavy metal (tungsten) will be used to absorb the photons with a good efficiency. The mask occupies a polar angle region of $0.15< \theta <0.2$. The front aperture of the mask needs to be minimized in the light of reducing the background. However, it has to let the core part of the incoming beam pass through. An aperture size of $r = 4.5$ cm was chosen. The conical mask is mechanically connected to a 10.36 cm-thick cylindrical mask of the same material in a hermetic manner. A doublet of final focus quadrupole magnets, QC1 and QC2, are implemented inside the mask. QC1 and QC2 are surrounded by a super-conducting solenoid magnet that compensates the detector solenoid field of 2 T.

Inside the conical mask, two kinds of detectors will be installed: a beam profile monitor (at 1 m from the IP), and a luminosity monitor of tungsten-scintillator sandwich type (at 1.63 m from the IP, covering $0.05 < \theta < 0.15$). A set of 20 cm-thick carbon mask is also implemented (0.5 m from the IP). The carbon mask is designed to absorb back-scattered low energy particles. The mask will be built as an "active" device which generates signals to veto scattered electrons/positrons at $\theta >0.05$ in combination with the luminosity monitor. They are considered important detector elements for studies of SUSY physics[7]. Around the interaction point there is a vertex detector of three layers. The present radius of innermost layer is 2.5cm. All the elements are installed in a support tube of 80cm inner radius in order to keep the relative

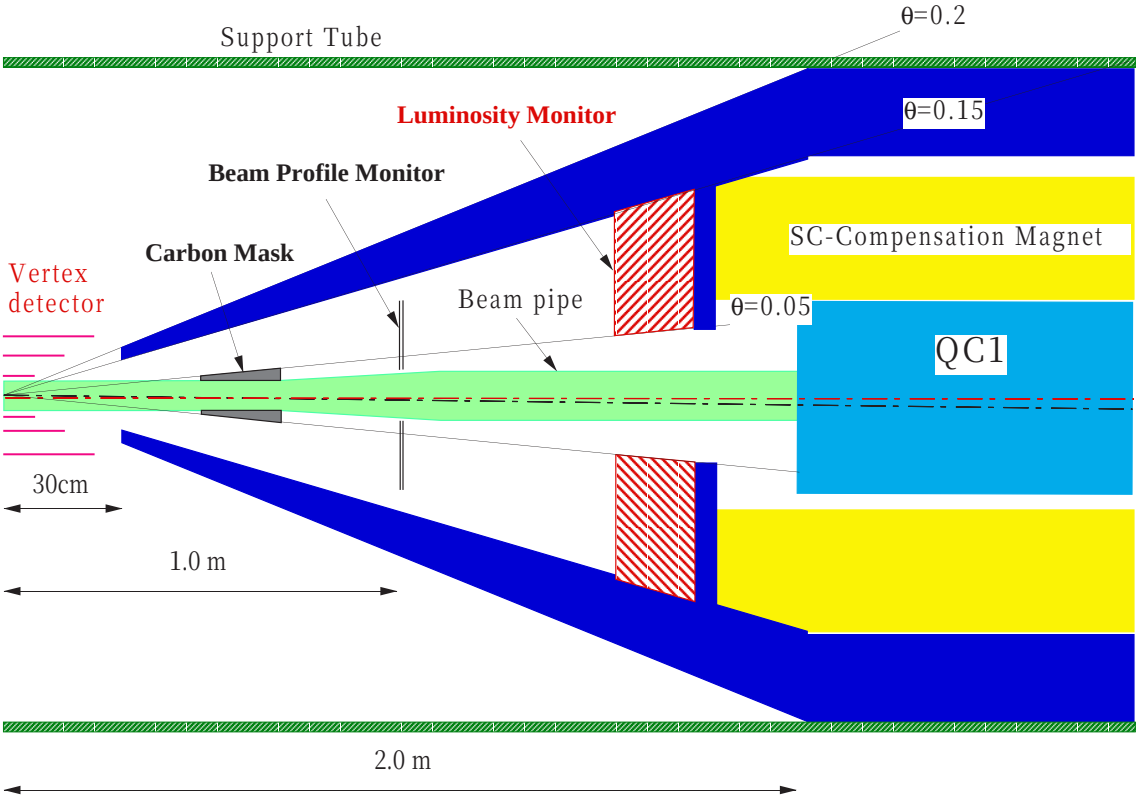

Figure 7: Schematic view of the interaction region for E_{cm} =0.5TeV.

position of the forward and backward QC1's within a few nm against a ground motion at the frequency of more than 10Hz[8]. This is very important for the stable luminosity.

Since this configuration and a required performance for detectors are strongly correlated to background conditions, we have investigated backgrounds in the detectors by using JIM (JLC detector simulation program) based on GEANT3.21. The highest hit density due to backgrounds is 3.6 hits/mm^2/train at the innermost layer of the vertex detector, which is marginal for the tolerable level. While the major backgrounds are electrons/positrons at the vertex detector, Xrays are dominant at central tracking region (r >30cm). The Xrays may produce a few thousand hits per train crossing in the central drift chamber(CDC) of CO_2/isobutane (90/10%) gas mixture with the present configuration[9]. It is desirable to reduce the hits by an order of magnitude for the better performance of CDC. So, further study is highly necessary. Also, neutron background contribution must be carefully investigated.

4 Detectors

A general purpose detector has been proposed in 1992 for JLC[1] and it is shown in Figure 8. All the major apparatuses are located inside of 2-tesla superconducting magnet in order to minimize materials between the central drift chamber and calorimeter. The angular coverage is $|\cos\theta|$ <0.98. The energy resolutions of the calorimeter (CAL) are $\sigma_E/\sqrt{E} = 15\%/\sqrt{E} \oplus 1\%$ and $\sigma_E/\sqrt{E} = 40\%/\sqrt{E} \oplus 2\%$ for electrons/photons and hadrons, respectively. Both the electromagnetic and hadronic calorimeters are sandwich counters consisting of layers of lead and plastic scintillators with tile fiber readout. The thickness of lead and scintillators shall be

optimized for the calorimeter to be compensating type, which has the same energy deposit for electromagnetic particles and hadrons. The momentum resolution of the central drift chamber (CDC) is $\sigma_{p_t}/p_t = 1.1\times10^{-4}p_t \oplus 0.1\%$. The chamber is a small cell type jet chamber comprizing super layers filled with a gas mixture of CO_2/isobutane(90/10%) for a good and uniform spatial resolution (100μm). The chamber must have about one hundred-thousand wires of 4.6 m long with well-controlled gravitational and electro-static sags. At the center of the detector very close to the interaction point, there is a vertex(CCD) detector (VTX), whose innermost radius is 2.5cm from the beam line, to tag bottom quarks. The impact parameter resolution is $\delta^2 = 11.4^2 + (28.8/p)^2/\sin^3\theta(\mu\mathrm{m}^2)$. Because of the severe background condition around the vertex detector, a radiation- hard CCD must be desired. The muon chamber (MDC) is located outside of the magnetic coil. It consists of 6 super layers of single-cell drift chambers, 4 of which are interleaved between iron yokes. The purpose is not a momentum measurement but a good muon identification for p >3.5 GeV with the spatial resolution of 500μm. The wires are 10m long so that they shall be supported in the middle to reduce the gravitational sag.

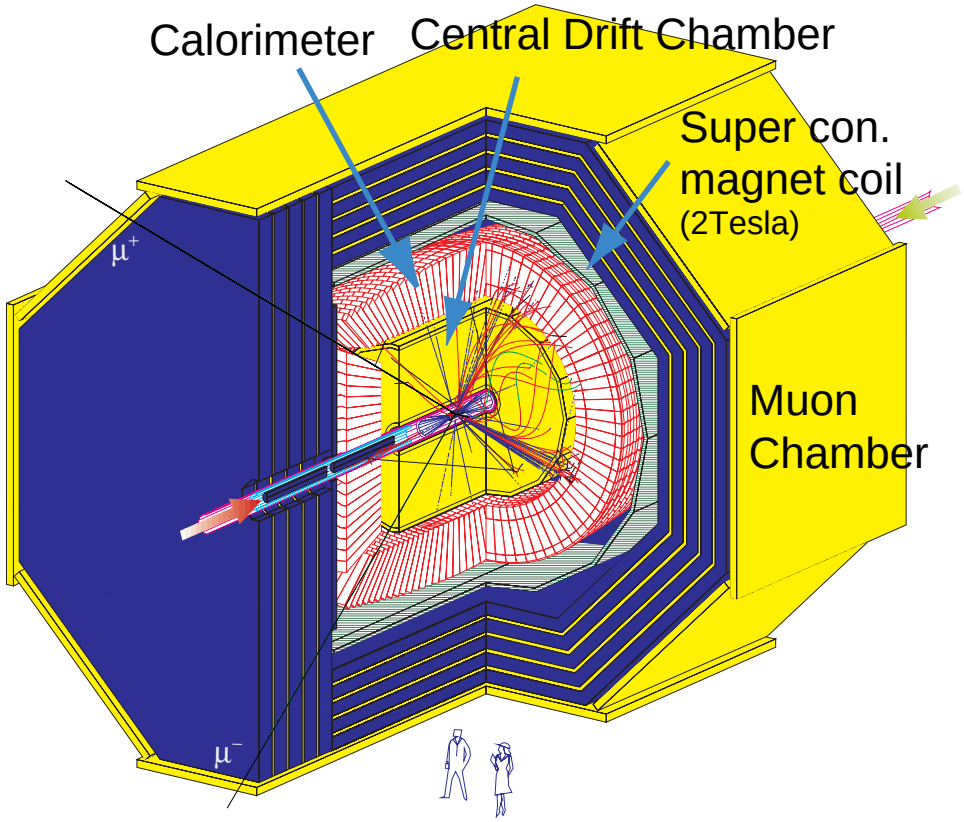

Figure 8: Schematic view of the JLC detector. The total volume is $16\times16\times16\mathrm{m}^3$, and it weighs 15,000 tons. A simulated event of Higgs boson production ($e^+e^- \to Zh$, $h \to b\bar{b}$, $Z \to \mu^+\mu^-$) is also superimposed for m_h=120GeV at $\sqrt{s}$=300GeV.

Recently, European and north American linear collider study groups proposed detectors for TESLA[10] and NLC[11], respectively. The major performance, type and size of these detectors are compared with those of JLC in Table 2. The radial sizes are approximately proportional to the detector solenoid-magnetic field (B) ranging from 2 to 6 tesla. All detectors have very

Table 2: Performance of proposed detectors(the barrel parts) for JLC, TESLA and NLC.

detector		JLC	TESLA	NLC-"S"	-"L"
magnet	B (tesla)	2	3	6	2
	size (m)	$9\phi\times$ 10	$6.5\phi\times$ 9.2	$2.3\phi\times$ 3.1	$8.2\phi\times$ 9.4
central	$\frac{\sigma_{P_t}}{P_t}$	$1.1\cdot10^{-4}P_t\oplus0.1\%$	$< 1.1\cdot10^{-4}P_t$	$1.6\cdot10^{-4}P_t$	$0.5\cdot10^{-4}P_t$
tracker	type	drift chamber	TPC	Si μ strips	TPC
	n, $\sigma(\mu$m)	100, 100.	118, 160.		140, 144.
	size (m)	$0.4 < r < 2.3$	$0.32 < r < 1.7$	$0.1 < r < 0.75$	$0.25 < r < 2.0$
		$\lvert z\rvert < 2.3$	$\lvert z\rvert < 2.8$	$\lvert z\rvert < 1.2$	$\lvert z\rvert < 3.0$
calorimeter					
electro-	$\frac{\sigma}{\sqrt{E}}(\%)$	$15/\sqrt{E}\oplus1$	$10/\sqrt{E}\oplus1$	$12/\sqrt{E}\oplus1$	$15/\sqrt{E}\oplus1$
magnetic	w/ scint.	tile:Pb	shashlik:Pb	Pb w/Si	Pb
	size (m)	$2.5 < r < 2.7$	$1.7 < r < 2.1$	$0.75 < r < 1.1$	$2.0 < r < 2.5$
		$\lvert z\rvert < 4.0$	$\lvert z\rvert < 2.8$	$\lvert z\rvert < 1.55$	$\lvert z\rvert < 3.5$
hadronic	$\frac{\sigma}{\sqrt{E}}(\%)$	$40/\sqrt{E}\oplus2$	$50/\sqrt{E}\oplus4$	$50/\sqrt{E}\oplus2$	$40/\sqrt{E}\oplus2$
	w/ scint.	tile:Pb	shashlik:Cu	Cu	Pb
	size (m)	$2.7 < r < 4.0$	$2.1 < r < 3.0$	$1.4 < r < 2.5$	$2.5 < r < 3.7$
		$\lvert z\rvert < 4.0$	$\lvert z\rvert < 3.3$	$\lvert z\rvert < 2.65$	$\lvert z\rvert < 4.7$
vertex	δ (μm)	$11.4\oplus\frac{28.8}{P\sin^{3/2}\theta}$	$10\oplus\frac{30}{P\sin^{3/2}\theta}$	$4.5\oplus\frac{5.5}{P\sin^{3/2}\theta}$	$10\oplus\frac{30}{P\sin^{3/2}\theta}$
detector	type	CCD	CCD or APS	CCD	CCD
	size (cm)	$2.5 < r < 7.5$	$2.5 < r < 10.$	$1.0 < r < 10.$	$2.5 < r < 10.$
		$\lvert z\rvert < 22.5$	$\lvert z\rvert < 30.^*$	$\lvert z\rvert < 12.5$	$\lvert z\rvert < 15.$

where, n is a number of measured points.
* including endcaps.

similar performances of momentum and calorimetric energy resolutions. NLC-"S" has a magnet coil inside of hadronic calorimeter, while the coils of other detectors are located outside of it. NLC-"S" is a compact detector with silicon micro-strips for the central tracker and tungsten-silicon pads for the electromagnetic calorimeter. Tightly confining the e^+e^- pairs along the beam line with very high magnetic field of 6 tesla, the radius of the first layer of vertex detector can decrease to 1cm at NLC-"S". TESLA and NLC-"L" employed a "wireless" drift chamber, time projection chamber(TPC), as the central tracker. For the dimension NLC-"L" is very similar to JLC, while TESLA is about 2/3 scaled JLC. To partially compensate the smaller size of hadron calorimeter, TESLA and NLC-"S" use copper(Cu) absorber instead of lead (Pb) for its shorter nuclear interaction length(λ); that is, a λ corresponds to 95% lateral contamination of hadronic shower.

5 Summary

The present JLC detector has been studied mainly by Japanese group. The detector concept may not be the same as the JLC detector in the ACFA working group. So the discussion should be open for any concept. Since this meeting is the first ACFA workshop on physics and detector

at the linear collider, we would like to list general issues to be discussed at a series of workshops.

1. Detector size: Detector size can be classified into two, that is, "large"(conventional) and "small"(compact). Dimensions of the central trackers are typically $4.6\phi\times4.6$ m(z) and $1.1\phi\times2.4$ m(z) for "large" and "small", respectively. The compact detector must use silicon μ strip or scintillation fiber tracker with higher magnetic field(B) because of $\sigma_p/p^2 \propto \sigma_x/BL^2\sqrt{n+2}$ where L is a level arm of trajectory measurement and n is the measurement points. These trackers are robust against the Xray background with less occupancy rate than usual drift chambers. Also final focus quadrupole magnet can be outside of the detector. On the other hand, the "large" detector has a better matching between charged tracks and calorimetric clusters, which is important for good energy resolution of the calorimeter. The central tracker is a "conventional" drift chamber such as a small-cell type jet chamber and time projection chamber. The above discussion is one of pros and cons in the choice of these two options.

2. Electromagnetic calorimeter: The energy resolutions of all proposed electromagnetic calorimeters range from $10\%/\sqrt{E}$ to $15\%/\sqrt{E}$ (Table 2), which are worse than those of crystal calorimeters such as CsI and $PbWO_4$ crystals. Do we need a better energy resolution for electromagnetic particles? One physics example is a measurement of two photon decay of Higgs($h\rightarrow\gamma\gamma$). Recent analysis of J.F. Gunion and P.C. Martin shows that $PbWO_4$ calorimeter (CMS type) can improve the measurement error of $\sigma\cdot BR(h\rightarrow\gamma\gamma)$ by more than 50% in $e^+e^-\rightarrow Zh$ at the optimized center-of-mass energy while it has 30% improvement in $e^+e^-\rightarrow Zh$ and $e^+e^-\rightarrow\nu_e\nu_e h$ at $\sqrt{s}$ =500GeV[12].

3. Hadron calorimeter: The hadron calorimeter of JLC detector is compensation type without offline correction. If the offline correction works, different type of calorimeter can be considered. Copper absorber may have better isolation of the clusters than lead absorber and crystals can be the electromagnetic calorimeter.

4. Vertex detector: The minimum radius of the vertex detector could decrease from 2.5 cm to 1 cm with higher magnetic field as NLC-"S". Is there any motivation to pursue the smaller radius? Under the background condition at linear colliders, the vertex detector must be pixel-type device and has only two options, that is, CCD and APS (active pixel sensor). In general, CCD has the best spatial resolution because of the thinner depleted region. However, it has less radiation hardness. The estimation of neutron background is a few 10^8 n/cm^2·year to be compared with the tolerable level of 10^9/cm^2. A fast readout (100MHz) is desired to transfer all the data of 10^8 channels at 150 Hz. Contrary, the major issue of APS is the spatial resolution which may be overcome by recent development[13].

5. Minimum veto angle: For SUSY studies such as stau pair production ($e^+e^-\rightarrow\tilde{\tau}^+\tilde{\tau}^-$), a calorimetric veto system is very important to identify the background of two photon process ($e^+e^-\rightarrow e^+e^-\tau^+\tau^-$)[7]. The minimum veto angle is 200 mrad outside of the mask (Figure 7). If the mask is activated, it can be 50 mrad including the luminosity monitor. Do we need a smaller veto angle than 50 mrad?

6. Intermediate tracker: There is a large empty space between the vertex detector(VTX) and the central drift chamber(CDC), that is, 7.5cm < r < 40cm, inside of 80cmϕ support tube. In this space an intermediate tracker can be installed to effectively link charged tracks between the VTX and the CDC. What performance is needed for it ? What kind of device is appropriate?

7. Forward tracker: It has been emphasized that the beam energy spread affects strongly on measurement of toponium spectrum as a function of $\sqrt{s}$[14]. If the energy spread (FWHM) exceeds 0.4 %, the spectrum start to depend on it. The typical energy spread is 0.5-1.0% in FWHM. For such a case, luminosity spectrum shall be measured as a function of $\sqrt{s}$ even within the energy spread. One possibility is to measure accolinearity angles of Bhabha events, which linearly depend on the energy difference between the initial electron and positron[15, 16]. So

the forward (backward) angular region is especially important for the high event rate. In order to measure the scattering angle precisely in this region, probably inside of the support tube, a forward tracker must be needed. What is the angular resolution ($\sigma_\theta < 1$mrad) ? Is it a μ strip detector?

9. Particle identification: There is no detector dedicated to a particle identification in all the proposed detectors. Is it needed? It is interesting that the gauge mediated SUSY model predicts stable charged particles as NLSP, which can penetrate detectors without decaying. For such heavy particles, dE/dX measurement in CDC is good enough ?

9. Good time resolution: Although the calculation of minijets has a large uncertainty, several minijet events may overlap with a signal event for a train crossing. Since one train consists of 85 bunches separating 1.4nsec, detectors with a good time resolution of O(1nsec) can resolve into a signal and minijets. The effect of the overlap has been studied to worsen the invariant mass resolution of two jets from 3.9GeV to 5.4GeV in $e^+e^- \to Zh$, $h \to$ 2jets when each signal is overlapped with a minijet[1]. Therefore, all the detectors , especially CDC and CAL, must have good time resolutions.

10. Trigger: No hardware trigger scheme has been considered because the collision frequency of JLC is 150Hz at most which is enough for sophisticated software trigger between the collisions. However, do we still need a hardware trigger?

11. Data acquisition: Data sizes of major detectors are listed for typical hadronic events in Table 3. Data size is dominated by CDC, and the maximum size is 12 Mbyte/event. All the detectors must be readout without writing the data on tapes at 150Hz.

Table 3: Data size and electronics of the JLC detector.

detector	total channels	typical data size	electronics
vertex	6×10^3	68 kbytes/bunch	flash ADC
CDC	1.8×10^4	12 Mbytes/event	flash ADC(500MHz,8bit)
CAL	3×10^4	30 kbytes/event	ADC
MDC	1.25×10^4	40 kbytes	TDC

Acknowledgments

I would like to thank the members of JLC physics and accelerator groups for usefull discussions. I also appreciate all the participants for their stimulative discussions during this workshop.

References

[1] JLC group, JLC-I(the green book),*KEK Report* 92-16, 1992.

[2] *The Final Report of the Subcommittee on Future Projects of High Energy Physics in Japan*, High Energy News Vol.17, May 1998. The report can be also obtained from a ftp-site of ftp://ftp/kek.jp/kek/HEPSC/final/.

[3] JLC Design Study Group: *JLC Design Study*, KEK Report 97-1, April 1997, see also ftp://lcdev.kek.jp/pub/DesignStudy/.

[4] I. Watanabe *et al.*: *$\gamma\gamma$ Collider as an Option of JLC*, KEK Report 97-17, March 1998.

[5] , Y. Namito, talk presented at the ISG3 (3rd meeting of the international study group), January 25-28, 1999, SLAC. The transparencies can be seen from a web site of http://www-project.slac.stanford.edu/lc/ilc/ISG_Meetings/ISG3/workgrp6.html.

[6] T. Tauchi and H. Hayashii, proceedings of Workshop on *Physics and Experiments with Linear e^+e^- Colliders(LCWS93)*, eds. F.A.Harris, S.L.Olsen, S.Pakvasa and X.Tata (World Scientific, Singapore, 1993), pp.745-753.

[7] M.M.Nojiri, K.Fujii and T.Tsukamoto, *Phys. Rev.* D **54**, 6756 (1996).

[8] S. Kanda, the same proceedings as [6], pp.758-761.

[9] The Xray-background estimation was wrong in the JLC design report[3], because Xrays of energies of <200keV were not simulated there.

[10] *Conceptual Design of a 500 GeV e^+e^- Linear Collider with Integrated X-ray Laser Facility*, DESY 1997-048, edited by R.Brinkmann et al. , May 1997.

[11] The NLC Design group, *Zeroth-order Design Report for the Next Linear Collider*, SLAC Report 474, May 1996. The recent activity can be seen from a home page of http://lcwws.physics.yale.edu/lc/america.html.

[12] J.F. Gunion and P.C. Martin, *Phys. Rev. Lett.* **78**, 4541 (1997).

[13] H. Yamamoto, in this proceeding of the first ACFA workshop on detector/physics at linear colliders.

[14] K. Fujii, T. Matsui and Y.Sumino, *Phys. Rev.* D **47**, 82 (1993).

[15] M.N. Frary and D.J. Miller, e^+e^- collisions at 500 GeV: the physics potential, ed. by P. Zerwas, DESY report 92-123A, 1992, p.379.

[16] N. Toomi *et al. Phys. Lett.* B **429**, 162 (1998).